ChemComm

# Carbon nanotube Encapsulated Metal selenide Nanostructures for Efficient Electrocatalytic Oxygen Evolution Reaction



| | |
|---|---|
| Journal: | *ChemComm* |
| Manuscript ID | CC-COM-05-2022-003026.R1 |
| Article Type: | Communication |
| | |

COMMUNICATION

# Carbon Nanotube Encapsulated Metal Selenide Nanostructures for Efficient Electrocatalytic Oxygen Evolution Reaction

Harish Singh[a], Wipula Liyanage[a] , and Manashi Nath[a*]

Received 00th January 20xx,
Accepted 00th January 20xx

DOI: 10.1039/x0xx00000x

**Nickel selenide nanowires were grown inside carbon nanotubes through in situ encapsulation via one-step chemical vapor deposition. These $NiSe_2$@CNT nanohybrids showed excellent electrocatalytic activity for water splitting with low overpotential of 260 mV at 10 mA/cm², high current density, and extended stability owing to synergistic effect between $NiSe_2$ and CNTs.**

Rapid population growth on a global scale, and over-exploitation of fossil fuels, has intensified the importance of identifying renewable and environmentally friendly sustainable energy sources. Over the past several decades major efforts have been made to explore clean and sustainable alternative sources of energy to meet such rising energy demands and reduce dependence on fossil fuel reserves. Among these, water electrolysis has been identified as an appealing technology for clean hydrogen generation that can mitigate the increasing global energy demands. The efficiency of water electrolysis is restricted by slow kinetics of the electron-intensive oxygen evolution reaction (OER) at the anode. A high-performance electrocatalyst is required to accelerate OER, lower the overpotential, and maximize energy conversion.

Conventionally, state-of-the-art electrocatalysts for OER are mostly based on precious metal oxides, such as those of ruthenium (Ru) and iridium (Ir), although their widespread applications are hindered by scarcity and high cost.[1,2] In recent years, earth-abundant pyrite-type transition metal dichalcogenides (TMDs) with the general formula, $MX_2$ ($M$= Co or Ni and $X$= Se or Te) has been identified as promising electrocatalysts for OER.[3,4] Ni has recently been utilized as an attractive element in the fabrication of anode materials for water electrolysis, due to low price, ample reserves, high electrochemical activity and the durability in highly alkaline medium.[5] Among various Ni-based compounds (e.g. oxides,[6] hydroxides,[7,8] sulfides,[9] phosphides,[10] and nitrides[11]), nickel selenides have shown significant promise for OER due to specific electronic structure, high electrical conductivity, low cost, and easy availability.[12] Various stoichiometries of nickel selenide has been explored as highly efficient OER electrocatalyst over the last few years. Nickel selenide can form with various stoichiometries, such as $Ni_{0.85}Se$/NiSe, $NiSe_2$, $Ni_3Se_4$, and $Ni_3Se_2$ each of which exhibits unique lattice structure. Among these $NiSe_2$ is of particular interest due to its intrinsic metallic properties as well as enhanced electrochemical activity of the Ni center, making it a suitable electrocatalyst.[13] Unlike pyrites such as $FeS_2$ or $NiS_2$, $NiSe_2$ is a paramagnetic Pauli metal with a resistivity less than $10^{-3}$ cm.[14] Such high conductivity is very advantageous for OER activity since it improves charge transfer within the catalytic grains.

Apart from high electrical conductivity of the catalyst grains, intergrain conductivity in the catalyst composite is also very crucial for improved electrocatalytic activity.[15–17] Moreover, poor electrical contact between catalysts and electrode also leads to poor stability, and the catalysts can be easily peeled off during oxygen evolution process. Hence, a common approach to increase conductivity of the catalyst composite involves using conducting carbon nanostructures as additive. The highly conductive multi-walled carbon nanotubes (MWCNTs) not only enable rapid charge transfer, but also provide routes for rapid ion transport and access to the electrolyte. Recently, Chen and co-workers have reported a series of studies on nickel selenide–CNTs composites synthesised through hydrothermal process which demonstrates surprisingly better performance for OER compared to support-free NiSe, $NiSe_2$ and $Ni_3Se_2$.[18] However higher onset potential of NiSe among all three nickel selenide catalysts limits use of these composites for efficient fuel cell application. Also, many advanced OER catalysts like these were synthesized using solvent-based hydrothermal techniques, which ultimately leads to secondary environmental pollution. In this communication we have reported a novel $NiSe_2$ nanorod encapsulated in MWCNT ($NiSe_2$@CNT) that was grown on graphite foil substrate through bottom-up method using high-temperature CVD technique. This $NiSe_2$@CNT nanostructure exhibited highly efficient OER activity for extended time period.

Department of Chemistry, Missouri University of Science and Technology, Rolla, MO 65409, USA.

Electronic Supplementary Information (ESI) available: Experimental and characterization details, Raman spectra of NiSe2@CNT, C1s XPS spectra of $NiSe_2$@CNT, PXRD of hydrothermally synthesized $NiSe_2$, LSV plots OF MWCNT and hydrothermally synthesized $NiSe_2$, comparison table of Nickel selenide-based OER catalysts and EIS parameters.

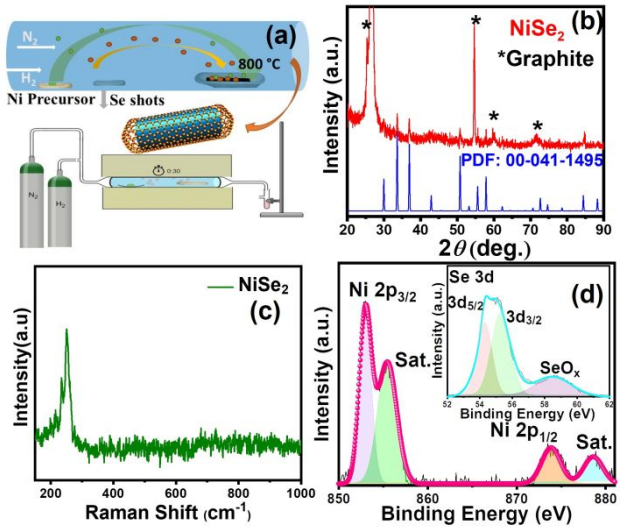


**Figure 1**. (a) Synthesis scheme of $NiSe_2$@CNT on graphite foil through CVD and *in situ* encapsulation. (b) PXRD of as deposited $NiSe_2$@CNT on graphite foil. (c) Raman spectra of as deposited $NiSe_2$@CNT. High resolution XPS spectra of (d) Ni, and Se (inset).

Volatile Ni-precursor, Ni-acetylacetonate along with Se was used to grow the $NiSe_2$. Pyrolysis of the carbon-rich acetylacetonate ligand led to *in situ* growth of MWCNT, while reaction between metal and selenium vapours led to formation of metal selenide inside the growing nanotubes on graphite foil substrate as shown in Figure 1(a). Interestingly, acetylacetonate functions as an appropriate source of C without the need for using any other hydrocarbon precursor, which increases purity of the product. It would be interesting to employ this kind of new synthesis strategy that would allow for extensive filling of the CNT channels with nanostructures while also making it amenable to scale-up and improving reproducibility. The properties of carbon nanotubes are highly dependent on the structural characteristics of CNTs, such as their diameter, level of filling in the core, and the presence of defects. Three-dimensional (3D) structures would undoubtedly significantly increase OER activity by exposing more accessible active sites from the external or inner surfaces.[19,20] CVD is a preferred and more efficient industrial technique for monitoring 2D and 3D nanomaterial growth and for modifying their properties as compared to other synthesis approaches. In addition, CVD is the most effective technique for homogeneous and continuous growth of thin films with very low defect density and high electro-conductivity.[21,22]

The PXRD patterns of the $NiSe_2$@CNT nanostructure hybrid showed characteristic diffraction peaks which matched well with the $NiSe_2$ standard diffraction pattern (PDF No. 00-041–1495) as shown in Figure 1(b). The absence of PXRD peaks for metallic Ni or excess Se from the metal precursors used in the CVD process indicates the high purity of the as-grown $NiSe_2$ on graphite foil substrate. Raman spectroscopy was used to examine local structure of the as-prepared $NiSe_2$@CNT composite electrode (Figure 1c), which confirmed composition of the nanostructure hybrid. Raman peaks were detected around 217 $cm^{-1}$ and 243 $cm^{-1}$, corresponding to the $A_g$ and $T_g$ modes of $NiSe_2$, respectively.[23] Characteristic Raman peaks corresponding to MWCNTs were also observed at 1338 $cm^{-1}$ (D-band) and 1584 $cm^{-1}$ (G-band) as shown in Figure S1. X-ray photoelectron spectroscopy (XPS) was used to elucidate chemical composition and changes in the electronic structure around the elements. Figure 1d and S2 represents high resolution XPS spectra of Ni 2p, Se 3d and C1s, respectively. In Figure 1d, the XPS spectra showed peaks at 856.8 and 874.6 eV corresponding to Ni $2p_{1/2}$ and Ni $2p_{3/2}$, respectively, and indicating presence of $Ni^{2+}$. The peaks at 862.1 and 880.4 eV are ascribed to the satellite structures. The existence of $Se^{2-}$ ions is supported by the two prominent peaks at 54.3 eV for Se $3d_{5/2}$ and 55.2 eV for Se $3d_{3/2}$. Furthermore, due to slight surface oxidation of Se, a shoulder peak was observed at 59.1 eV which can be assigned to Se–O. The morphology of the $NiSe_2$@CNT nanostructure hybrid was studied with electron microscopy. Scanning electron microscopy (SEM) revealed a high yield of CNTs with length exceeding several micrometres, as illustrated in Figure 2(a). The detailed morphology of $NiSe_2$@CNT composite was studied through high-resolution transmission electron microscopy (HRTEM) which showed the extent of $NiSe_2$ filling within the MWCNT as shown in Figure 2(b-e). HRTEM images exhibited lattice fringes in the $NiSe_2$ filling with a layer spacing of 0.268 nm corresponding to (210) lattice planes of $NiSe_2$, indicating high degree of crystallinity of the encapsulated $NiSe_2$ nanostructure. The average filling length of $NiSe_2$ was estimated to be in the range of 400 – 600 nm determined by studying several

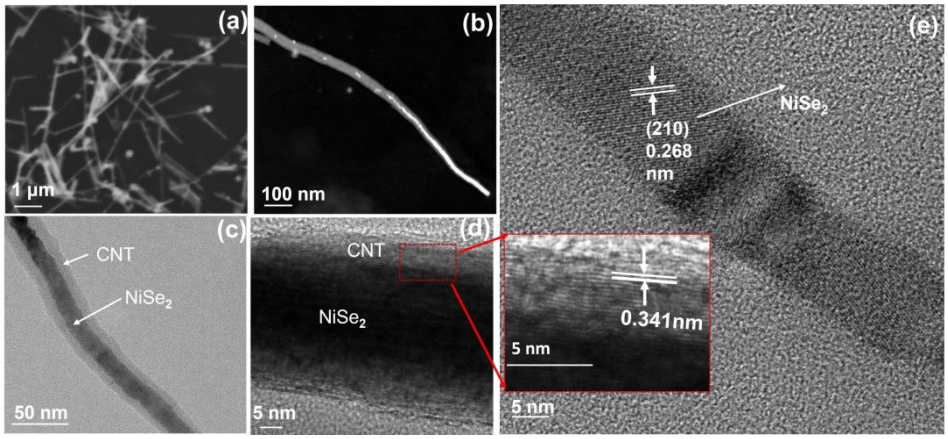


Figure 2. (a) SEM of $NiSe_2$@CNT electrode. (b) Dark field and (c) bright field TEM image of $NiSe_2$@CNT showing extensive filling. (d) TEM image of CNT filled with $NiSe_2$ showing diffused interface. (e) High-resolution TEM image showing characteristic d-spacing of $NiSe_2$ in the core region and d-spacing of CNT (inset, from region selected from figure 2d}.

$NiSe_2$@CNT structures. It must be noted that TEM revealed majority of the MWCNTs to be $NiSe_2$ filled.

The OER electrocatalytic performance of as-prepared $NiSe_2$@CNT composite electrode (on graphite) was investigated in $O_2$-saturated 1 M KOH. Figure 3(a) illustrates the LSV polarization curves of $NiSe_2$@CNT which was compared with that of $RuO_2$. The LSV plots clearly showed that $NiSe_2$@CNT had better OER catalytic activity compared to $RuO_2$. Bare graphite foil and graphite foil heated at 800 °C was also studied as control substrates. As expected, the graphite foils did not show any activity for OER confirming that observed activity for the composite electrode was due to $NiSe_2$@CNT hybrid nanostructure. The effect of MWCNT was also investigated by comparing the activity of $NiSe_2$@CNT with that of $NiSe_2$ synthesized through hydrothermal method ($NiSe_2$-HD, characterized through PXRD as shown in Figure S3, which showed peaks corresponding to pure $NiSe_2$, (PDF-00-041-1495)) and with commercially available MWCNT. The results indicate that $NiSe_2$@CNT has highest activity toward OER, requiring 260 mV overpotential to achieve a current density of 10 mA/cm$^2$, whereas $NiSe_2$-HD, $RuO_2$ and MWCNT required 300, 380 and 410 mV under similar conditions. As can be seen in Figure S4, hydrothermally synthesized $NiSe_2$ and MWCNT sample showed higher onset potential and lower conductivity than the CVD synthesized $NiSe_2$@CNT sample which confirms the synergistic effect of $NiSe_2$@CNT catalyst that was directly grown over the graphite foil and produced a binder-free film. The hydrothermally synthesized $NiSe_2$ was assembled on the carbon cloth electrode by using Nafion as binder, which limited exposure of the active sites and introduced contact resistance between electrode and catalysts, leading to subdued catalytic performance. Also, as synthesized $NiSe_2$@CNT showed excellent catalytic activity as compared to most of the recently reported nickel-based catalysts (Table S1). The OER kinetics were examined using the Tafel plots as shown in inset of Figure 3(b). Clearly, $NiSe_2$@CNT exhibited favourable OER kinetics, as measured by small Tafel slope of 82.5 mV dec$^{-1}$, which was significantly less than that of benchmark $RuO_2$ electrocatalyst (114.9 mV dec$^{-1}$). The lower Tafel slope of $NiSe_2$@CNT indicates a greater enhancement in OER kinetics since the current density increased steeply as the overpotential increased. Multistep chronoamperometry plot of the $NiSe_2$@CNT electrode in shown in Figure 3b, where current density was increased sequentially from 10 to 50 mA cm$^{-2}$ after every 15 hours while the overpotential was measured at each constant current density. These chronoamperometry tests were performed at applied potentials of 1.49, 1.51 and 1.58 V to achieve current density of 10, 20 and 50 mA cm$^{-2}$, respectively. $NiSe_2$@CNT demonstrated excellent stability at different applied potential for prolonged time with minimal performance degradation as shown in Figure 3(c) which revealed negligible shift in the polarization curves after 45 hours of multistep chronoamperometry, implying that $NiSe_2$@CNT catalyst has exceptional mechanical robustness and mass transport capabilities for OER under alkaline conditions. As shown in Figure 3d, multistep chronoamperometry measurements were also performed at various constant applied potentials to evaluate the robustness of $NiSe_2$@CNT electrode. The potential steps were varied from 1.44 V to 1.62 V vs RHE (ascending and descending) where current density at each step was measured for ~2 h. Enhancement of the Ni oxidation peak was observed after long term chronoamperometry of $NiSe_2$@CNT composite electrodes as shown in inset of Figure 3c. Such pre-oxidation has been observed commonly with majority of Ni based electrocatalysts containing $Ni^{2+}$ and attributed to local site oxidation of Ni(II) to Ni(III). Figure 3(e) represents the ECSA of as synthesised $NiSe_2$@CNT catalyst, wherein, higher ECSA values usually result in better active site exposure and OER catalysis. The ECSA of $NiSe_2$@CNT electrode was obtained using the double layer capacitance in non-Faradaic region obtained from cyclic voltammetry (CV) plots, as shown in inset of Figure 3(e). Corresponding capacitive current at 0.15 V vs SCE were recorded from each CV at different scan rates in 1 M KOH to determine the ECSA. The ECSA of as prepared electrode was estimated to be 6.825 cm$^2$. The turnover frequency (TOF) of $NiSe_2$@CNT sample was

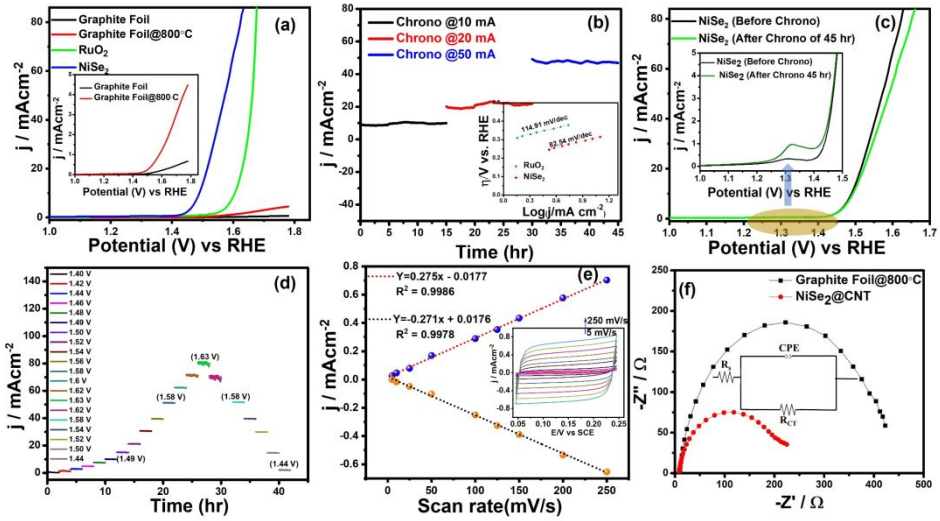


**Figure 3**. OER electrocatalytic performance of $NiSe_2$@CNT. (a) LSVs measured in 1 M KOH at a scan rate of 10 mV s$^{-1}$. (b) Chronoamperometry at different applied potential. Inset shows the Tafel plot of $NiSe_2$@CNT and $RuO_2$. (c) LSV of $NiSe_2$@CNT before and after 45 h of chronoamperometry. (d) Multistep chronoamperometry at different applied potential steps (ascending and descending). (e) Cyclic voltammograms measured at different scan rates for $NiSe_2$@CNT. Inset shows the anodic and cathodic currents measured as function of different scan rates. (f) Nyquist impedance plots of $NiSe_2$@CNT. Inset represents equivalent circuit model used for AC impedance fitting.

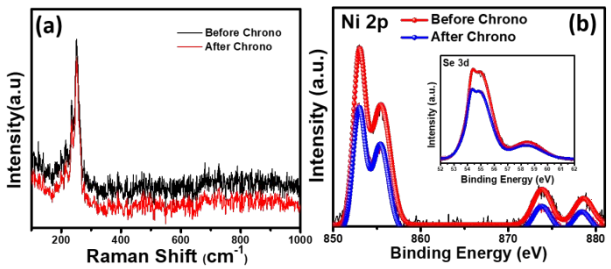


**Figure 4.** (a) Raman and (b) XPS of $NiSe_2$@CNT after 45 h chronoamperometry.

determined using standard method as described in the supporting information. At a potential of 1.58 V and current density of 50 mA/cm$^2$, the TOF for $NiSe_2$@CNT was estimated to be 0.39 $s^{-1}$. Typically, higher TOF indicates improved catalytic activity, confirming the highly efficient electrocatalytic activity of $NiSe_2$@CNT composite. The Faradaic efficiency of $NiSe_2$@CNT catalysts for OER activity was estimated to be 100 % using the water displacement method. EIS measurements were used to determine the basis for the superior OER activity of the $NiSe_2$@CNT catalyst composite. The EIS plot (Figure 3f) could be fitted to the equivalent circuit (Table S2) and the charge-transfer resistance ($R_{CT}$) was estimated to be 209 Ω. Low Rct for the $NiSe_2$@CNT composite compared to bare graphite foil substrate heated at 800°C (416 Ω) indicates facile charge transfer at the electrode-electrolyte interface due to synergistic effect of the highly conductive $NiSe_2$@CNT electrode. Compositional stability of the catalyst was analyzed by measuring the XPS and Raman spectra after 45 hours of OER. The Raman spectrum (Figure 4a) and XPS pattern (Figure 4b) were found to be almost unchanged compared to the pristine sample indicating the $NiSe_2$@CNT catalyst composite was indeed stable for extended period.

The enhanced OER activity of $NiSe_2$@CNT nanohybrid architecture indicates that the introduction of MWCNTs lower the overpotential and can improve the electrical conductivity which favours fast charge-transfer in the electrocatalytic process. Such intimate chemical fusion between the catalytic $NiSe_2$ and conducting MWCNT is more favourable than physical admixture (obtained by mixing $NiSe_2$ grains with MWCNTs) which shows reduced charge transfer across grain boundaries. The core-shell like $NiSe_2$@CNT nanohybrid, on the other hand, is expected to have enhanced charge transfer across domain interface due to intermixing of lattice planes at the interface (as seen in TEM images, Figure 2(d)), which is intrinsic to chemical fusion. Due to confinement effects induced by the surrounding CNT walls, it was inferred that $NiSe_2$ entrapped within carbon nanotube channel not only exhibited outstanding catalytic performance but also showed superior stability under harsh oxidative condition of water oxidation. The encapsulation of CNTs around metal chalcogenide is an intriguing concept that can increase conductivity and charge transfer, protect from catalyst leaching and peeling off as well as retain robust performance for maintaining steady catalytic efficiency.

In summary, the OER catalytic performance of $NiSe_2$@CNT was most strongly influenced by intergrowth of $NiSe_2$ within MWCNT, synthesized by CVD process. $NiSe_2$@CNT nanohybrid also showed superior stability and significantly enhanced performance, with an overpotential of 260 mV at 10 mA $cm^{-2}$ current density and Tafel slope of 82.5 mV $dec^{-1}$. Additionally, this study establishes a new synthesis technique for designing nanohybrids with highly efficient metal chalcogenide nanorods wrapped within MWCNT for fuel cell applications.

## Acknowledgements

The authors would like to acknowledge NSF (DMR1710313, CHE2155175) for financial support and MRC for equipment usage.

## Conflicts of interest

There are no conflicts to declare.

## Notes and references

1 Takahiro Naito, Tatsuya Shinagawa, Takeshi Nishimoto and Kazuhiro Takanabe, Inorg. Chem. Front., 2021, 8, 2900–2917.
2 Y. Li, Y. Sun, Y. Qin, W. Zhang, L. Wang, M. Luo, H. Yang and S. Guo, Adv. Energy Mater., 2020, 10, 1903120.
3 M. Nath, U. De Silva, H. Singh, M. Perkins, W. P. R. Liyanage, S. Umapathi, S. Chakravarty and J. Masud, ACS Appl. Energy Mater., 2021, acsaem.1c01438.
4 A. T. Swesi, J. Masud and M. Nath, Energy Environ. Sci., 2016, 9, 1771–1782.
5 K. S. Bhat and H. S. Nagaraja, Mater. Res. Innov. 2019, 25, 29–52.
6 A. G. Hufnagel, A. K. Henß, R. Hoffmann, O. E. O. Zeman, S. Häringer, D. Fattakhova-Rohlfing and T. Bein, Adv. Mater. Interfaces, 2018, 5, 1–12.
7 M. Gao, W. Sheng, Z. Zhuang, Q. Fang, S. Gu, J. Jiang and Y. Yan, J. Am. Chem. Soc., 2014, 136, 7077–7084.
8 P. Ding, C. Meng, J. Liang, T. Li, Y. Wang, Q. Liu, Y. Luo, G. Cui, A. M. Asiri, S. Lu and X. Sun, Inorg. Chem., 2021, 60, 12703–12708.
9 O. Mabayoje, A. Shoola, B. R. Wygant and C. B. Mullins, ACS Energy Lett., 2016, 1, 195–201.
10 P. W. Menezes, A. Indra, C. Das, C. Walter, C. Göbel, V. Gutkin, D. Schmeißer and M. Driess, ACS Catal., 2017, 7, 103–109.
11 M. Shalom, V. Molinari, D. Esposito, G. Clavel, D. Ressnig, C. Giordano and M. Antonietti, Adv. Mater., 2014, 26, 1272–1276.
12 L. Lv, Z. Li, Y. Ruan, Y. Chang, X. Ao, J. G. Li, Z. Yang and C. Wang, Electrochim. Acta, 2018, 286, 172–178.
13 M. Z. Xue and Z. W. Fu, Electrochem. commun., 2006, 8, 1855–1862.
14 M. Z. Xue and Z. W. Fu, Electrochem. commun., 2006, 8, 1855–1862.
15 A. Saxena, W. Liyanage, J. Masud, S. Kapila and M. Nath, J. Mater. Chem. A, 2021, 9, 7150–7161.
16 X. Wang, A. Dong, Y. Hu, J. Qian and S. Huang, Chem. Commun., 2020, 56, 10809–10823.
17 L. Chai, Z. Hu, X. Wang, L. Zhang, T. T. Li, Y. Hu, J. Pan, J. Qian and S. Huang, Carbon N. Y., 2021, 174, 531–539.
18 S. Chen, J.-L. Mi, P. Zhang, Y.-H. Feng, Y.-C. Yong and W.-D. Shi, J. Phys. Chem. C, 2018, 122, 26096–26104.
19 T. Thippani, S. Mandal, G. Wang, V. K. Ramani and R. Kothandaraman, RSC Adv., 2016, 6, 71122–71133.
20 M. S. Ahmed, B. Choi and Y.-B. Kim, Sci. Rep., 2018, 8, 2543.
21 B. Liu, M. Fathi, L. Chen, A. Abbas, Y. Ma and C. Zhou, ACS Nano, 2015, 9, 6119–6127.
22 S. Mishra, K. Song, K. C. Ghosh and M. Nath, ACS Nano, 2014, 8, 2077–2086.
23 H. Zhou, Y. Wang, R. He, F. Yu, J. Sun, F. Wang, Y. Lan, Z. Ren and S. Chen, Nano Energy, 2016, 20, 29–36.
24 Y. Qiu, X. Zhang, H. Han, Z. Liu, J. Liu and X. Ji, J. Power Sources, 2021, 499, 229941.
25 Y. Qiu, Z. Feng, X. Ji and J. Liu, Int. J. Hydrogen Energy, 2021, 46, 1501–1508.